Available online at www.sciencedirect.com
SCIENCE DIRECT®
International Journal of Solids and Structures 42 (2005) 139–158
INTERNATIONAL JOURNAL OF SOLIDS and STRUCTURES
www.elsevier.com/locate/ijsolstr

# Principle of analysis of brittle-plastic rock mass

H. Zheng [a,*], D.F. Liu [a], C.F. Lee [b], X.R. Ge [c]

[a] *Department of Hydroelectric Engineering, College of Civil & Hydroelectric Engineering, China Three Gorges University, College Road 8, Yi Chang 443002, China*
[b] *Department of Civil Engineering, The University of Hong Kong, Hong Kong*
[c] *Institute of Rock and Soil Mechanics, Chinese Academy of Sciences, Wuhan 430071, China*

Received 16 January 2004; received in revised form 28 June 2004
Available online 11 September 2004

**Abstract**

Based upon Il'yushin's postulate and the plastic potential theory, a procedure for calculating the abrupt change in stresses from the peak strength surface to the residual strength surface is proposed. The stability criterion for a brittle-plastic body loaded proportionally is presented. Finally, three examples have been solved analytically and numerically, including an engineering example of the steep rock slope of a shiplock system for the Three Gorges hydroelectric power project in China.


*Keywords:* Brittle-plasticity; Rock mass; Stability

## 1. Introduction

The advent of the "stiff" testing machines with advanced control systems has made possible the study of the stress–strain behavior of brittle-plastic hard rocks. Great progresses have been made in the study of the brittle rocks in the last two decades. However, up to now, there has been no mechanical model that is capable of describing all aspects of deformation of brittle rocks.

So far, several mechanical models that can be adopted to simulate the deformation of brittle rocks have distinct concerns. For example, the main advantage of the micromechanical models (see Wong, 1982; Fredrich and Wong, 1986; Fredrich et al., 1989; Kemeny and Cook, 1991) is the ability to describe the microstructural microcrack kinetics and to reproduce some macroscopic behaviors of brittle rock

* Corresponding author. Tel.: +86 71 763 92635; fax: +86 71 763 95328.
*E-mail address:* hzheng@ctgu.edu.cn (H. Zheng).

0020-7683/$ - see front matter © 2004 Elsevier Ltd. All rights reserved.
doi:10.1016/j.ijsolstr.2004.06.050

specimens in test. A quite complete review on micromechanics was given by Kemeny and Cook (1991). If the process of the strain localization is emphasized, several conceptually different approaches for modeling of localized deformation are available, including the use of the Cosserat continuum (de Borst, 1991; Muhlhaus and Vardoulakis, 1987), the non-local theory (Pijaudier-Cabot and Bazant, 1987), gradient-dependent formulations (de Borst and Muhlhaus, 1992, 1993; Roy et al., 2003), strong discontinuity approaches (Regueiro and Borja, 2000; Wells and Sluys, 2001, etc.). Bardet (1990), Pietruszczak and Xu (1995), present quite comprehensive reviews for two development phases till 1990 and 1995, respectively. In addition, the statistical method (Krajcinovic and Mastilovic, 1999; Mastilovic and Krajcinovic, 1999, etc.) seems to be a promising way to describe the deformation of the brittle rock.

On the other hand, if main concerns focus on the failure zone's distribution and the degree of deformation in practice, some simpler approaches based on the classical continuum theory, such as Zhang and Subhash (2001), Hajiabdolmajida et al. (2002), Lo and Lee (1973), as well as continuous damage models (e.g., Krajcinovic and Vujosevic, 1998; Ju, 1989; Etienne et al., 1998; Chiarelli et al., 2003), are also practical. Though there might exist mesh dependency in some aspects to a certain extent using these approaches, estimation of the failure zone's distribution and the degree of failure are quite accurate. In many situations, the failure zone's distribution and the degree of failure, for example, the excavation disturbed zones (EDZ), are sufficient to decide the lengths of anchors and/or bolts to be designed to reinforce the failure zones. Therefore, these approaches based on the classical continuum theory have still been adopted in engineering computations.

The failure mechanism of brittle rocks is stated in Wawersik and Brace (1971), Steif (1984), Sammis and Ashby (1986), Martin and Chandler (1994) and Atkinson (1984), and Litewka and Debinski (2003). Based upon the phenomenological description, it is generally recognized that a salient feature of a brittle-plastic material is that it displays an abrupt post-peak drop in stress on the stress–strain ($\sigma$–$\varepsilon$). In other words, when a point in a stress space is loaded from its initial elastic state to the peak strength surface (PSS), stress will drop abruptly to the residual strength surface (RSS). It is this discontinuous change of the yield surface in the stress space that causes difficulties in an analysis. The determination of this abrupt drop in stress from PSS to RSS has been a key issue in the finite element analysis of a brittle-plastic rock mass. To date, a number of computational procedures have been proposed, involving different assumptions and hence leading to different results.

In this paper, a procedure based on the generalization of the classical theory of plasticity for determining the abrupt change in stresses for a brittle-plastic material is proposed. The proposed method does not require any parameters for describing the microcracks of the rock. Derived from the classical theory of plasticity, the proposed concepts and methodology are more readily accepted by engineers, and it is also convenient to implement in finite element analysis.

The abrupt changes in stress of a brittle material may result in unstable behavior for the majority of rock structures. In this paper, a formulation on the stability of a brittle body loaded proportionally is presented. Finally, the effectiveness of the proposed methods is examined using two simple examples where the analytical solutions are available. The proposed methods are also applied to analyze the steep rock slope of a shiplock system of the Three Gorges hydroelectric project in China.

## 2. Brittle-plastic rock

In general, there are two main types of post-peak $\sigma$–$\varepsilon$ behavior of brittle rocks as shown in Fig. 1. If the declining segment of curve no. I or no. II is very near to the perpendicular line AB under certain range of confining pressures, this type of rock can be regarded as a brittle-plastic rock to be studied in this paper. An idealized model is shown in Fig. 2, in which $\bar{\sigma}$ and $\bar{\varepsilon}$ are, respectively, the equivalent stress and equivalent strain corresponding to a certain yield criterion. Lo and Lee (1973) discussed this model in the stability

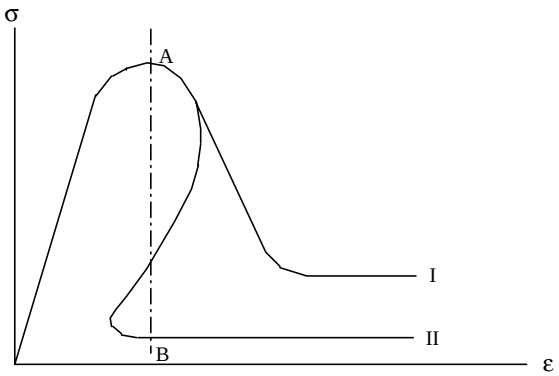


Fig. 1. Two basic types of full process curves.

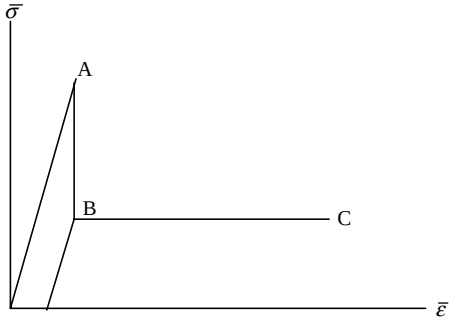


Fig. 2. Brittle-plastic model.

analysis of slopes. At present, this model has been applied in many cases, for example, Hajiabdolmajida et al. (2002), Wang and Dussealt (1994). This model is described as follows. When a point in the rock is loaded from its initial elastic state to its peak strength at point A, it will drop rapidly to the point B on the residual strength line BC. After this, continuous loading will lead to a $\sigma$–$\varepsilon$ relation that follows on line BC and cause plastic deformation. Otherwise, unloading at some point on BC will result in some elastic responses.

For unstable materials, Il'yushin has proposed a thermodynamic postulate (Chen and Han, 1988), which is more extensive than Drucker's postulate and is stated as follows: After any element in a body undergoes a closed cycle of strain, the work done by stress in the closed cycle of strain is not negative. If a material satisfies this postulate, a complete system of the elasto-plastic constitutive theory for the material can be formulated.

For a system with one degree of freedom as shown in Fig. 3(a), obviously, any closed cycle of strain far from point A would make the work done by stress not negative. Now taking a closed cycle of strain near point A, the corresponding stress path is D → A → B → E → F. The magnitude of the work done by stress along each segment is the area enclosed by the segment, the two perpendicular lines passing the two end points of the segment and the $\varepsilon$ axis. The sign of the work done is the same as $d\varepsilon$ (assuming that stress is positive here). Therefore the work done is positive along DA and BE, zero along AB, and negative along EF. After a complete closed cycle of strain, the pure work done by stress is the area of the polygon DABEF and its value is positive. Therefore, any brittle-plastic material can be included in Il'yushin's postulate.

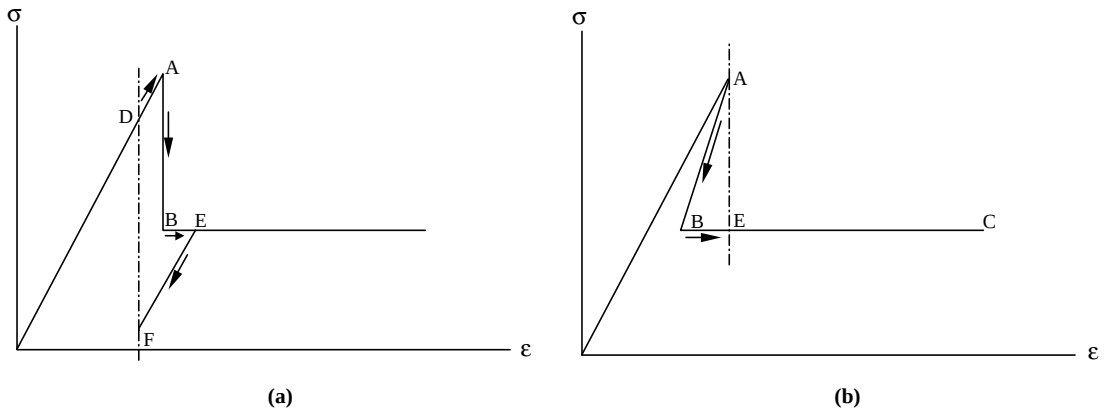


Fig. 3. Work done by stress in one cycle of strain: (a) brittle-plastic material, (b) material of type II.

However, the situation is not true for rock of curve no. II characteristic, particularly when we take a closed cycle of strain at point A as shown in Fig. 3(b). The corresponding stress path is $A \rightarrow B \rightarrow E$. The magnitude of the work done by stress along this path is equal to the area of the triangle ABE, and its value is negative. Therefore a rock with the characteristic of curve no. II does not satisfy Il'yushin's postulate.

## 3. Limitation of classical theory of plasticity for softening material

In order to evade the indeterminacy of the stress-drop in brittle-plastic materials, some researchers would consider brittle damage as a continuous strain-softening process as shown in Fig. 4. However this approach does not agree with the deformation characteristics of brittle-plastic rocks, because for brittle-plastic rocks the process from PSS to RSS is not gradual but abrupt, and any stress state during dropping is also not recoverable. Obviously, the continuous strain-softening model cannot adequately describe these phenomena of brittle-plastic rocks.

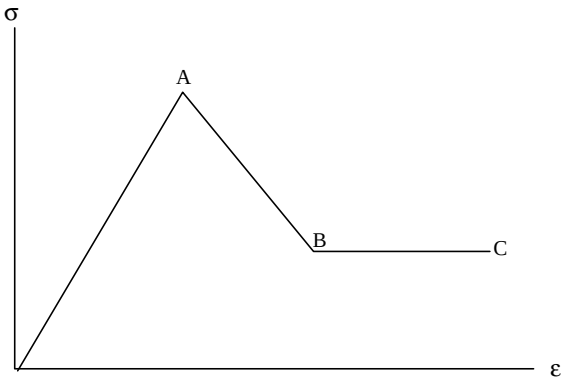


Fig. 4. The continuous strain softening model.

Furthermore, even if the continuous strain-softening model is adopted, it is impossible to carry out the computation by taking the real softening segment under the classical elasto-plasticity framework, because the classical plasticity theory has a limitation to the rate of the strain softening. In the following, we will point that the classical constitutive integration is of significance only if the rate of softening is relatively low.

Suppose the yield surface of rock is

$$F(\boldsymbol{\sigma}, w_{\mathrm{p}}) = 0, \tag{1}$$

where $w_{\mathrm{p}}$ is the plastic work, defined as

$$w_{\mathrm{p}} = \int \boldsymbol{\sigma}^{\mathrm{T}} \mathrm{d}\boldsymbol{\varepsilon}_{\mathrm{p}}. \tag{2}$$

For the case of plastic loading, the stress increments are given by (Zienkiewicz and Taylor, 1991)

$$\mathrm{d}\boldsymbol{\sigma} = \boldsymbol{D}_{\mathrm{ep}}\mathrm{d}\boldsymbol{\varepsilon}, \tag{3.1}$$

$$\boldsymbol{D}_{\mathrm{ep}} = \boldsymbol{D} - \boldsymbol{D}_{\mathrm{p}}, \quad \boldsymbol{D}_{\mathrm{p}} = \frac{1}{M}\boldsymbol{D}\frac{\partial F}{\partial \boldsymbol{\sigma}}\left(\frac{\partial F}{\partial \boldsymbol{\sigma}}\right)^{\mathrm{T}}\boldsymbol{D}. \tag{3.2}$$

Here, $\boldsymbol{D}_{\mathrm{ep}}$, $\boldsymbol{D}$ and $\boldsymbol{D}_{\mathrm{p}}$ are the matrices in plasticity constitutive theory. The notation in this paper is consistent with the monograph by Zienkiewicz and Taylor (1991). The real number $M$ is defined as

$$M \equiv A + \left(\frac{\partial F}{\partial \boldsymbol{\sigma}}\right)^{\mathrm{T}}\boldsymbol{D}\frac{\partial F}{\partial \boldsymbol{\sigma}} \tag{3.3}$$

and the real number $A$ as

$$A \equiv -\frac{\partial F}{\partial w_{\mathrm{p}}}\boldsymbol{\sigma}^{\mathrm{T}}\frac{\partial F}{\partial \boldsymbol{\sigma}}. \tag{3.4}$$

For hardening materials, the real number $A > 0$, for ideal plastic materials $A = 0$, and for softening materials $A < 0$. But in the case of softening, $A$ must satisfy

$$|A| < \left(\frac{\partial F}{\partial \boldsymbol{\sigma}}\right)^{\mathrm{T}}\boldsymbol{D}\frac{\partial F}{\partial \boldsymbol{\sigma}}, \quad A < 0. \tag{4}$$

In fact, if $|A| = (\frac{\partial F}{\partial \boldsymbol{\sigma}})^{\mathrm{T}}\boldsymbol{D}\frac{\partial F}{\partial \boldsymbol{\sigma}}$ and $A < 0$, then $M = 0$. This makes $\boldsymbol{D}_{\mathrm{ep}}$ indeterminant.

If $|A| < (\frac{\partial F}{\partial \boldsymbol{\sigma}})^{\mathrm{T}}\boldsymbol{D}\frac{\partial F}{\partial \boldsymbol{\sigma}}$ and $A < 0$, then $M < 0$. Hence, $\boldsymbol{D}_{\mathrm{ep}}$ can be written as

$$\boldsymbol{D}_{\mathrm{ep}} = \boldsymbol{D} + \frac{1}{|M|}\boldsymbol{d}_F\boldsymbol{d}_F^{\mathrm{T}} \quad \text{with} \quad \boldsymbol{d}_F = \frac{\partial F}{\partial \boldsymbol{\sigma}}.$$

Since

$$\mathrm{d}\boldsymbol{\sigma} = \left(\boldsymbol{D} + \frac{1}{|M|}\boldsymbol{d}_F\boldsymbol{d}_F^{\mathrm{T}}\right)\mathrm{d}\boldsymbol{\varepsilon} \tag{5}$$

pre-multiplying Eq. (5) with $(\mathrm{d}\boldsymbol{\varepsilon})^{\mathrm{T}}(\neq 0)$ leads to

$$(\mathrm{d}\varepsilon)^{\mathrm{T}}\mathrm{d}\boldsymbol{\sigma} = (\mathrm{d}\boldsymbol{\varepsilon})^{\mathrm{T}}\boldsymbol{D}\mathrm{d}\boldsymbol{\varepsilon} + \frac{1}{|M|}[(\mathrm{d}\boldsymbol{\varepsilon})^{\mathrm{T}}\boldsymbol{d}_F]^2.$$

Then $(\mathrm{d}\boldsymbol{\varepsilon})^T\mathrm{d}\boldsymbol{\sigma} > 0$ can be derived from the fact that $\boldsymbol{D}$ is positive definite, but this contradicts the definition of softening. Therefore, for any softening material, a constitutive relationship can be determined only if its softening rate satisfies inequality (4).

Taking the Drucker–Prager's material with isotopic hardening as an example, the equation for the yield surface is given by

$$F(\boldsymbol{\sigma}, w_{\mathrm{p}}) = \alpha I_1 + \sqrt{J_2} - \kappa = 0 \tag{6}$$

in which $\alpha = \alpha(w_{\mathrm{p}})$, $\kappa = \kappa(w_{\mathrm{p}})$. Let $\alpha' = \frac{\mathrm{d}\alpha}{\mathrm{d}w_{\mathrm{p}}}$, $\kappa' = \frac{\mathrm{d}\kappa}{\mathrm{d}w_{\mathrm{p}}}$, we have

$$\left(\frac{\partial F}{\partial \boldsymbol{\sigma}}\right)^{\mathrm{T}} \boldsymbol{D} \frac{\partial F}{\partial \boldsymbol{\sigma}} = 9\alpha^2 K + G$$

where

$$K = \frac{E}{3(1-2v)}, \quad G = \frac{E}{2(1+v)}$$

and

$$A = -\frac{\partial F}{\partial w_{\mathrm{p}}} \boldsymbol{\sigma}^{\mathrm{T}} \frac{\partial \boldsymbol{F}}{\partial \boldsymbol{\sigma}} = \kappa(\kappa' - \alpha' I_1)$$

$\kappa' - \alpha' I_1 > 0$ means hardening and $\kappa' - \alpha' I_1 = 0$ means perfect plasticity, while $\kappa' - \alpha' I_1 < 0$ represents softening, but the limit to the softening rate is

$$|\kappa(\kappa' - \alpha' I_1)| < 9\alpha^2 K + G. \tag{7}$$

If the variation of $\alpha$ to $w_{\mathrm{p}}$ is ignored, i.e., $\alpha' = 0$, we have

$$\left|\frac{\mathrm{d}\kappa^2}{\mathrm{d}w_{\mathrm{p}}}\right| < 18\alpha^2 K + 2G. \tag{7.1}$$

For a Drucker–Prager's material, if its rate of strain softening satisfies Eq. (7) or (7.1), the material can be considered to be a continuous strain softening material. Otherwise, we should neglect the softening process and regard the material as a brittle-plastic material.

It should be noted that it is rather prone to be in danger in practice to regard brittle-plastic materials as continuous strain-softening materials.

## 4. Stress changes in a brittle-plastic rock

Suppose that $F(\sigma) = 0$ and $f(\boldsymbol{\sigma}) = 0$ represent PSS and RSS, respectively and a point is loaded from an initial elastic state to the point A on PSS, as shown in Fig. 5. If the loading condition is satisfied,

$$L = \left(\frac{\partial F}{\partial \boldsymbol{\sigma}}\right)^{\mathrm{T}} \boldsymbol{D}\, \mathrm{d}\boldsymbol{\varepsilon} > 0, \tag{8}$$

there will be an abrupt drop in stresses from the point A to the point B on RSS. There are at least three procedures for determining point B in the stress space in available finite element procedures, as shown in Fig. 6. In this figure, $B_1$ is determined based on the assumption that the center of the circle after dropping is kept invariant. $B_2$ is determined based on the assumption that the distance of dropping in the stress space would be shortest. $B_3$ is determined based on the assumption that the confining pressure $\sigma_1$ after dropping is kept invariant. Among these procedures the first method seems to be the most popular one. Wan et al. (1992) also proposed a procedure based on normal projection from B on RSS. Obviously, solutions from different methods lead to different results. In the following, we will present another method for determining the point B based on the plastic potential theory.

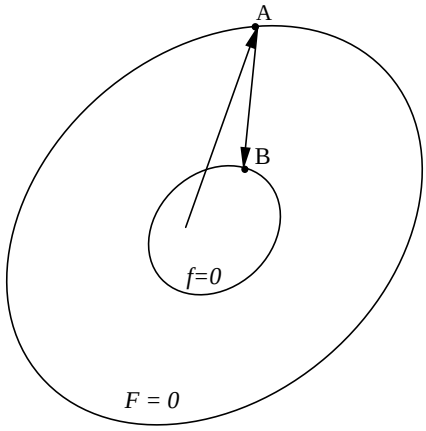


Fig. 5. Diagram of stress-dropping.

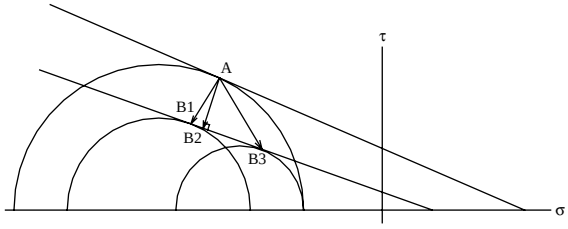


Fig. 6. Three typical kinds of hypotheses on stress-dropping.

Because of the brittleness of rock, the yield surface has a discontinuous change in the stress space, correspondingly, finite increments of plastic strains $\Delta\varepsilon_{ij}^{p}$ will be generated. Moreover, since brittle-plastic rock satisfies Il'yushin's postulate, we can therefore consider that the direction of the plastic strain increment vector at dropping will still accord with the plastic potential theory. For the sake of simplicity, we use the associated flow rule in the following. As a matter of fact, there is no essential difficult in applying the non-associated flow. In this case, we have

$$\Delta\varepsilon_{ij}^{p} = \Delta\lambda \left.\frac{\partial F}{\partial \sigma_{ij}}\right|_{A}, \tag{9}$$

where $\Delta\lambda$ is the plastic flow factor. Since

$$\Delta\varepsilon_{ij} = \Delta\varepsilon_{ij}^{e} + \Delta\varepsilon_{ij}^{p}. \tag{10}$$

Based on the triaxial testing of brittle materials of the standard model shown in Fig. 2, the change in the axial strain $\Delta\varepsilon_z = 0$. Thus, the changes in the circumferential and the radical strain $\Delta\varepsilon_\theta = \Delta\varepsilon_r = -v\Delta\varepsilon_z = 0$. Because the principle strain $\varepsilon_1$, $\varepsilon_2$ and $\varepsilon_3$ are equal to $\varepsilon_z$, $\varepsilon_r$ and $\varepsilon_\theta$, respectively, it can be considered that $\Delta\varepsilon_{ij} = 0$ during the process of stress dropping from PSS to RSS in general cases. Therefore, we have

$$\Delta\varepsilon_{ij}^{e} = -\Delta\varepsilon_{ij}^{p}. \tag{11}$$

Using

$$\Delta\sigma_{ij} = D_{ijkl}\Delta\varepsilon_{kl}^{e} \tag{12}$$

and substituting (9) and (11) into (12) leads to

$$\Delta\sigma_{ij} = \sigma_{ij}^{\mathrm{B}} - \sigma_{ij}^{\mathrm{A}} = -\Delta\lambda D_{ijkl}\left.\frac{\partial F}{\partial\sigma_{kl}}\right|_{\mathrm{A}} = -\Delta\lambda\tau_{ij}^{\mathrm{A}}. \tag{13}$$

Therefore

$$\sigma_{ij}^{\mathrm{B}} = \sigma_{ij}^{\mathrm{A}} - \Delta\lambda\tau_{ij}^{\mathrm{A}}, \tag{14}$$

where

$$\tau_{ij}^{\mathrm{A}} = D_{ijkl}\left.\frac{\partial F}{\partial\sigma_{kl}}\right|_{\mathrm{A}}. \tag{15}$$

As for $\Delta\lambda$, considering the stress $\sigma_{ij}^{\mathrm{B}}$ after dropping is on PSS, i.e.,

$$f(\sigma_{ij}^{\mathrm{B}}) = f(\sigma_{ij}^{\mathrm{A}} - \Delta\lambda\tau_{ij}^{\mathrm{A}}) = 0. \tag{16}$$

The numerical solution to Eq. (16) is trivial for any yielding surface. In the following, we will take Drucker–Prager's criterion for rock and Mohr–Coulomb's criterion for rock joints as examples and provide the procedures for determining $\Delta\lambda$.

Equations of PSS and RSS of rock with Drucker–Prager's form are, respectively,

$$F(\boldsymbol{\sigma}) = \alpha_0 I_1 + \sqrt{J_2} - \kappa_0 = 0, \tag{17.1}$$

$$f(\boldsymbol{\sigma}) = \alpha_r I_1 + \sqrt{J_2} - \kappa_r = 0, \tag{17.2}$$

where $\alpha_0$, $\kappa_0$ and $\alpha_r$, $\kappa_r$ represent strength parameters of PSS and RSS, respectively. From Eq. (16), we can derive that $\Delta\lambda$ is one of two roots of the following quadratic equation with one unknown quantity:

$$a\lambda^2 + b\lambda + c = 0 \tag{18.1}$$

in which

$$a = [\alpha_r I_1(\boldsymbol{\tau}^{\mathrm{A}}) - \kappa_r]^2 - J_2(\boldsymbol{\tau}^{\mathrm{A}}) = (9\alpha_0\alpha_r K)^2 - G^2 < 0; \quad c = [\alpha_r I_1(\boldsymbol{\sigma}^{\mathrm{A}}) - \kappa_r]^2 - J_2(\boldsymbol{\sigma}^{\mathrm{A}});$$
$$b = s^{\mathrm{A}} t^{\mathrm{A}} - 2\alpha_r I_1(\boldsymbol{\tau}^{\mathrm{A}})[\alpha_r I_1(\boldsymbol{\sigma}^{\mathrm{A}}) - \kappa_r] = 2G\sqrt{J_2(\boldsymbol{\sigma}^{\mathrm{A}})} - 18\alpha_0\alpha_r K[\alpha_r I_1(\boldsymbol{\sigma}^{\mathrm{A}}) - \kappa_r];$$

where $\boldsymbol{s}^{\mathrm{A}}$ and $\boldsymbol{t}^{\mathrm{A}}$ are the deviatoric tensors of $\boldsymbol{\sigma}^{\mathrm{A}}$ and $\boldsymbol{\tau}^{\mathrm{A}}$, respectively. Because the discriminant of Eq. (18.1)

$$b^2 - 4ac = [18\alpha_0\alpha_r K\sqrt{J_2(\boldsymbol{\sigma}^{\mathrm{A}})} - 2G(\alpha_r I_1(\boldsymbol{\sigma}^{\mathrm{A}}) - \kappa_r)]^2 > 0.$$

Eq. (18.1) must have two different roots:

$$\lambda_1 = f(\boldsymbol{\sigma}^{\mathrm{A}})/(9\alpha_0\alpha_r K + G) > 0,$$
$$\lambda_2 = (\alpha_r I_1(\boldsymbol{\sigma}^{\mathrm{A}}) - \kappa_r - \sqrt{J_2})/(9\alpha_0\alpha_r K - G)$$

Obviously, $\Delta\lambda$ can be taken from

$$\Delta\lambda = \begin{cases} \min(\lambda_1, \lambda_2) & \text{if } \lambda_2 > 0, \\ \lambda_1 & \text{if } \lambda_2 \leqslant 0. \end{cases} \tag{18.2}$$

Now, we can write respectively equations for PSS and RSS of the joint using Mohr–Coulomb's criterion as

$$F(\boldsymbol{\sigma}) = (\tau_{s1}^2 + \tau_{s2}^2)^{1/2} + m_0\sigma_n - c_0 = 0 \tag{19.1}$$

and

$$f(\boldsymbol{\sigma}) = (\tau_{s1}^2 + \tau_{s2}^2)^{1/2} + m_r\sigma_n - c_r = 0, \tag{19.2}$$

where $(\tau_{s1}, \tau_{s2})$ are shear stress components perpendicular to each other on the joint surface, $c_0$, $m_0(=tg\phi_0)$ and $c_r$, $m_r(=tg\phi_r)$ are strength parameters of PSS and RSS, respectively.

In general, the deformation in a rock joint might not be brittle but softening gradually. However, as stated in the preceding section, when the softening rate of strain of the joint is relatively large, we should neglect the softening process and regard it as a brittle process. In this case, $\Delta\lambda$ can be determined by means of the similar procedure

$$\Delta\lambda = f(\boldsymbol{\sigma}^{\mathrm{A}})/(k_{\mathrm{s}} + m_0 m_r k_{\mathrm{n}}), \tag{20}$$

where $k_{\mathrm{s}}$, $k_{\mathrm{n}}$ are the shear stiffness and the normal stiffness of the joint, respectively.

## 5. Stability criteria for brittle-plastic deformation

The stability of structures in brittle-plasticity rock is of significant engineering interest. Dems and Mroz (1985) provided a solution based on the sensitivity formulation, Liu and Xu (1989) put forward a formulation of the disturbed and damaged surface. These formulations were all used for obtaining solutions for relatively simple structures based on the maximum tensile stress criterion.

Taking into account the characteristics of a brittle-plastic body, we will now present the differential formulation of the stability of the body, which is based on damage zone expansion.

Let the region of rock in study be denoted by $\Omega$. Suppose that the traction $T_i(\boldsymbol{x},t)$ on $S_\sigma$ and the body force $b_i(\boldsymbol{x},t)$ in $\Omega$ are increased in the same proportion during the loading process, i.e., there exist the following decompositions:

$$\begin{aligned} T_i(\boldsymbol{x},t) &= \psi(t) T_{i0}(\boldsymbol{x}), \quad \boldsymbol{x} \in S_\sigma, \\ b_i(\boldsymbol{x},t) &= \psi(t) b_{i0}(\boldsymbol{x}), \quad \boldsymbol{x} \in \Omega, \end{aligned} \tag{21}$$

where $T_{i0}(\boldsymbol{x})$ and $b_{i0}(\boldsymbol{x})$ are known distribution functions of the traction and body force, respectively. $\psi(t)$ is the load multiplier, a monotonically increasing function, in which $t$ is only a measuring parameter of the loading process and is not related to any real time.

When $\psi(t)$ is equal to $\psi_{\mathrm{e}}$, the load multiplier of the elastic limit, the structure starts to have brittle damage. Suppose that $\Omega_{\mathrm{d}}$ and $\Omega_{\mathrm{c}}$ represents the damaged zone and the intact zone, respectively, corresponding to the load multiplier $\psi(t)(\geqslant\psi_{\mathrm{e}})$. Write the maximum external diameter of $\Omega_{\mathrm{d}}$ as $l(t)$:

$$l(t) = \mathrm{Max}_{\boldsymbol{x},\boldsymbol{y}\in\Omega_{\mathrm{d}}} \|\boldsymbol{x} - \boldsymbol{y}\|. \tag{22}$$

Obviously, for given distributions of loads $T_{i0}(\boldsymbol{x})$ and $b_{i0}(\boldsymbol{x})$ during the stage of stable deformation, there is a one-to-one correspondence between $l$ and $\psi$:

$$l(t) = L(\psi(t)), \quad (\psi(t) \geqslant \psi_{\mathrm{e}}) \tag{23.1}$$

or

$$\psi(t) = \Psi(l(t)), \quad (l(t) \geqslant 0). \tag{23.2}$$

Here, $L(\cdot)$ and $\Psi(\cdot)$ are two known functions. When $\psi(t)$ is equal to or exceeds $\psi_b$, the multiplier of the limit load, even if $\psi(t)$ does not change, the damaged zone $\Omega_{\mathrm{d}}$ would continue to expand. Therefore, we can consider the stability criterion as

$$\frac{\mathrm{d}\psi}{\mathrm{d}l} \begin{cases} > 0 \text{ stable state}, \\ = 0 \text{ critical state}, \\ < 0 \text{ unstable state}. \end{cases} \tag{24}$$

We denote by $\Gamma_d$ the interface surface between the damaged zone $\Omega_d$ and the intact zone $\Omega_c$. $\Gamma_d^c$ is the side of $\Gamma_d$ belonging to $\Omega_c$. In general, the condition on $\Gamma_d^c$, $F(\boldsymbol{\sigma}(\boldsymbol{x})) = 0$, $\boldsymbol{x} \in \Gamma_d^c$, can be used to form (23.1) or (23.2).

In principle, the above stability criterion applies only to simple structures under action of proportional loads. For general structures under action of complex load types, the critical loads are determined through iteration of the finite element analysis. This process has been stated in detail in many monographs on the non-linear finite element methods.

## 6. Numerical examples

### 6.1. Example 1. Expansion of a thick-walled cylinder

Consider a brittle-plastic thick-walled cylinder subjected to an internal pressure $p$ with the internal and external radius $a$ and $b$, respectively. For simplicity, the material is assumed to obey the Tresca's criterion. Applying such a simple criterion can still demonstrate some essentials of brittle-plastic deformation from the following discussion. The peak and residual tensile strength are given by $\sigma_b^0$ and $\sigma_b$, respectively. We will restrict our discussions to the stress solution.

#### 6.1.1. Elastic solution

When $p$ is smaller, we have the elastic solution (i.e. Lame's solution, Ajit and Sarva, 1991)

$$\sigma_\theta = \frac{pa^2}{b^2 - a^2}\left(1 + \frac{b^2}{r^2}\right), \quad \sigma_r = \frac{pa^2}{b^2 - a^2}\left(1 - \frac{b^2}{r^2}\right). \tag{25}$$

Substituting the above equations into the equation of PSS

$$F(\boldsymbol{\sigma}) = \sigma_\theta - \sigma_r - \sigma_b^0 = 0$$

and taking $r = a$, we have the elastic limit load

$$p_e = \frac{1}{2}\left(1 - \frac{a^2}{b^2}\right)\sigma_b^0. \tag{26}$$

#### 6.1.2. Brittle-plastic solution

If $p \geqslant p_e$, an enlarging plastic zone spreads outwards from the inner surface. Write the radius of the plastic zone as $c$. In the plastic zone, $\sigma_\theta$ and $\sigma_r$ should satisfy the following equations:

$$\begin{cases} \frac{d\sigma_r}{dr} - \frac{\sigma_\theta - \sigma_r}{r} = 0 \\ \sigma_\theta - \sigma_r - \sigma_b = 0 \\ \sigma_r|_{r=a} = -p \end{cases} \quad a \leqslant r \leqslant c. \tag{27}$$

Solving the above problem, we have

$$\sigma_\theta = \sigma_b\left(1 + \ln\frac{r}{a}\right) - p, \quad \sigma_r = \sigma_b \ln\frac{r}{a} - p \quad (a \leqslant r \leqslant c). \tag{28}$$

We may now use Lame's solution (25) to obtain stresses in the elastic zone

$$\sigma_\theta = \frac{p_c c^2}{b^2 - c^2}\left(1 + \frac{b^2}{r^2}\right), \quad \sigma_r = \frac{p_c c^2}{b^2 - c^2}\left(1 - \frac{b^2}{r^2}\right) \quad (c \leqslant r \leqslant b), \tag{29}$$

where $-p_c$ is the value of $\sigma_r$ in Eq. (28) at $r = c$ (i.e., $\Gamma_d$)

$$p_c = -\sigma|_{r=c-0} = p - \sigma_b \ln\frac{c}{a}. \tag{30}$$

*6.1.3. Limit load*

Obviously, on the surface $\Gamma_d^c$ (i.e., $r = c + 0$), the peak strength criterion should be satisfied:

$$F(\sigma) = (\sigma_\theta - \sigma_r)|_{r=c+0} - \sigma_b^0 = 0.$$

Substituting Eq. (29) and (30) into the above equation leads to a relationship between $p$ and $c$:

$$p = \sigma_b \ln\frac{c}{a} + \frac{1}{2}\left(1 - \frac{c^2}{b^2}\right)\sigma_b^0. \tag{31}$$

From the differential formulation (24) on stability, we can know that in the critical state

$$\frac{\mathrm{d}p}{\mathrm{d}c} = \frac{\sigma_b}{c} - \frac{\sigma_b^0}{b^2}c = 0.$$

Hence, the limit radius of the plastic zone can be obtained:

$$c_b = b\sqrt{\sigma_b/\sigma_b^0}. \tag{32}$$

Now, what the brittle-plastic deformation is different from the ideal elasto-plastic deformation is that under the condition of the ideal elasto-plastic deformation, as long as any elastic zone exists, the structure will be able to resist further expansion of the plastic zone. However, for brittle-plastic structures, such as in this example, when expansion of the plastic zone reaches a certain amount, even though some elastic zones still exist, the structure would collapse.

Moreover, an interesting phenomenon can be observed from the example. For a brittle-plastic thick-walled cylinder of a given external diameter $b$, $c_b$ is a characteristic size of the cylinder. If the inner radius $a \geqslant c_b$, that means the cylinder is thinner, once $p$ increases to the elastic load $p_e$, the cylinder would collapse before the damaged zone emerges. If $a < c_b$, the critical load $p_b$ can be obtained by substituting $c_b$ into Eq. (31). Therefore

$$p_b = \begin{cases} p_e & \text{if } a \geqslant c_b, \\ \frac{1}{2}(\sigma_b^0 - \sigma_b) + \sigma_b \ln\frac{b}{a}\sqrt{\sigma_b/\sigma_b^0} & \text{if } a < c_b. \end{cases} \tag{33}$$

It can be proved easily that

$$p_s < p_b < p_s^0 \quad \text{if } a < c_b, \tag{34}$$

where $p_s$ (or $p_s^0$) is the plastic limit load when regarding the cylinder as an ideal elastio-plastic material with the limit tensile strength $\sigma_b$ (or $\sigma_b^0$) (Chen and Han, 1988)

$$p_s = \sigma_b \ln\frac{b}{a} \quad \text{and} \quad p_s^0 = \sigma_b^0 \ln\frac{b}{a}. \tag{35}$$

In fact, considering if $x > 0$ then $1 + \ln x < x$, we have

$$p_b = \frac{1}{2}\left[\sigma_b^0 - \sigma_b\left(1 + \ln\frac{\sigma_b^0}{\sigma_b}\right)\right] + \sigma_b \ln\frac{b}{a} > \frac{1}{2}\left(\sigma_b^0 - \sigma_b\frac{\sigma_b^0}{\sigma_b}\right) + \sigma_b \ln\frac{b}{a} = p_s.$$

As for the right of inequality (34), we still have

$$p_b < \frac{1}{2}(\sigma_b^0 - \sigma_b) + \sigma_b^0 \ln\frac{b}{a}\sqrt{\sigma_b/\sigma_b^0} = \frac{1}{2}\left[\sigma_b^0\left(1 + \ln\frac{\sigma_b}{\sigma_b^0}\right) - \sigma_b\right] + \sigma_b^0 \ln\frac{b}{a} < \frac{1}{2}\left(\sigma_b^0\frac{\sigma_b}{\sigma_b^0} - \sigma_b\right) + \sigma_b^0 \ln\frac{b}{a} = p_b^0$$

Let $\sigma_b \to \sigma_b^0$, the above result tends to the solution of an ideal elasto-plastic problem.

### 6.2. Example 2. A circular tunnel in deep depth

Suppose that a circular tunnel of the radius $a$ is subjected to the supporting force $p$ and the uniform confining pressure $q$. The rock is homogeneous and brittle-plastic Mohr–Coulomb material. $C_0$, $\varphi_0$ and $C$, $\varphi$ represent the peak strength parameters and the residual parameters, respectively. The volume force is neglected. Considering the supporting force $p$ is much less than the confining pressure $q$, we regard that the plastic deformation surrounding the tunnel is caused by $q$.

#### 6.2.1. Elastic solution

When $q$ is relatively small, the elastic solution of the problem was given by Ajit and Sarva (1991):

$$\sigma_r = -q - (p-q)\frac{a^2}{r^2}, \quad \sigma_\theta = -q + (p-q)\frac{a^2}{r^2}. \tag{36}$$

Because of $\sigma_\theta < \sigma_r$, PSS takes the form

$$F(\boldsymbol{\sigma}) = n_0\sigma_r - \sigma_\theta - \sigma_c^0 = 0 \tag{37}$$

in which

$$n_0 = \frac{1+\sin\varphi_0}{1-\sin\varphi_0}, \quad \sigma_c^0 = \frac{2C_0}{1-\sin\varphi_0}. \tag{37.1}$$

Substituting (36) into (37) and considering $q \gg p$, we have the elastic limit confining pressure

$$q_e = \frac{1}{2}[\sigma_c^0 + (n_0+1)p]. \tag{38}$$

#### 6.2.2. Brittle-plastic solution

If $q \geqslant q_e$, the plastic zone will expand progressively from the tunnel's surface with the increasing $q$. In the plastic zone, $\sigma_r$ and $\sigma_\theta$ is the solution of the boundary value problem

$$\begin{cases} \frac{d\sigma_r}{dr} - \dfrac{\sigma_\theta - \sigma_r}{r} = 0 \\ f(\boldsymbol{\sigma}) = n\sigma_r - \sigma_\theta - \sigma_c \quad (a \leqslant r < b). \\ \sigma_r|_{r=a} = -p \end{cases} \tag{39}$$

Here, $b$ is the radius of the plastic zone

$$n = \frac{1+\sin\varphi}{1-\sin\varphi}, \quad \sigma_c = \frac{2C\cos\varphi}{1-\sin\varphi}. \tag{39.1}$$

From (39), we have

$$\begin{cases} \sigma_r = \dfrac{\sigma_c}{n-1} - \left(p + \dfrac{\sigma_c}{n-1}\right)\left(\dfrac{r}{a}\right)^{n-1} \\ \sigma_\theta = \dfrac{\sigma_c}{n-1} - n\left(p + \dfrac{\sigma_c}{n-1}\right)\left(\dfrac{r}{a}\right)^{n-1} \end{cases} \quad (a \leqslant r \leqslant b). \tag{40}$$

It can be seen that stresses in the plastic zone do not depend on the magnitude of the confining pressure $q$.

Applying Eq. (36), we can write out the stress in the elastic zone

$$\begin{cases} \sigma_r = -q - (p_b - q)\dfrac{b^2}{r^2} \\ \sigma_\theta = -q + (p_b - q)\dfrac{b^2}{r^2} \end{cases} \quad (r \geqslant b). \tag{41}$$

Here, $-p_b$ is the value of $\sigma_r$ in Eq. (40) at $r = b$, i.e., $\Gamma_d$

$$p_b = -\sigma_r|_{r=b-0} = \left(p + \frac{\sigma_c}{n-1}\right)\left(\frac{b}{a}\right)^{1-(1/n)} - \frac{\sigma_c}{n-1}. \tag{42}$$

Considering that the peak strength criterion should be satisfied on the interface $\Gamma_d^c$, $r = b + 0$

$$F(\boldsymbol{\sigma}) = (n_0\sigma_r - \sigma_\theta)|_{r=b+0} - \sigma_c^0 = 0 \tag{43}$$

substituting (41) and (42) into Eq. (43), the radius of the plastic zone can be obtained:

$$b = a\left(\frac{(n_0+1)\sigma_c + (n-1)(2q - \sigma_c^0)}{(n_0+1)[(n-1)p + \sigma_c]}\right)^{1/(n-1)}. \tag{44}$$

Because of $\frac{dq}{db} > 0$, according to Eq. (24), the circular tunnel is always stable for any confining pressure.

### 6.3. Example 3. An example of engineering application—a large rock excavation for the Three Gorges Project

When completed in 2008, the Three Gorges Project (TGP) will feature the largest power generating station of the world, with an installed generating capacity of 18,000 MW. Its other main function is flood control for the middle and lower reaches of the Yangzte River in Central China. Numerous disastrous floods have occurred along these parts of the Yangzte River Basin in history, often involving thousands of casualties and rendering millions of people homeless.

Since the Yangtze River is a major waterway for Central China, it is important to maintain the navigation capacity of the river after the TGP is completed. Fig. 7 shows the layout of the navigation facilities for the project, consisting of a permanent shiplock, a shiplift and a temporary shiplock, all located on the North shore of the Yangzte River at the dam site. The permanent shiplock is designed as a two-way, five-step flight system, with each navigation chamber dimensioned at $280 \times 34 \times 5$ m (length × width × minimum water depth). The shiplift is designed as a vertical hoisting type with a ship container sized at $120 \times 18 \times 3.5$ m. The temporary shiplock is schemed for use during the construction period with an effective chamber size of $240 \times 24 \times 4$ m.

The navigation facilities are constructed by deep excavation into the bedrock and the maximum excavation depths are 173.5, 140 and 86 m for the permanent shiplock, the shiplift and the temporary shiplock, respectively. The dominant rock type is plagioclase granite, which is divided into four zones according to the degree of weathering, viz., completely weathered (IV), highly weathered (III), moderately weathered (II), slightly weathered and fresh (I). Benches are left during excavation and are usually 15 m high and 5 m wide with a slope of 1 (vertical) to 1 (horizontal) for the completely and highly weathered zones, 1–0.5 for the moderately weathered zones, and 1–0.3 or vertical for the slightly weathered and fresh zones. The

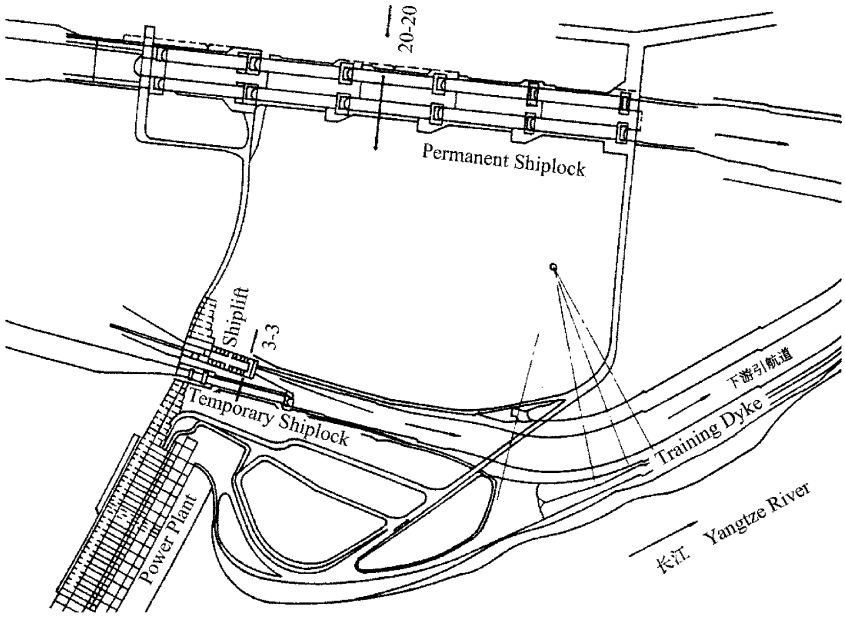


Fig. 7. The layout of the navigation facilities for the TGP.

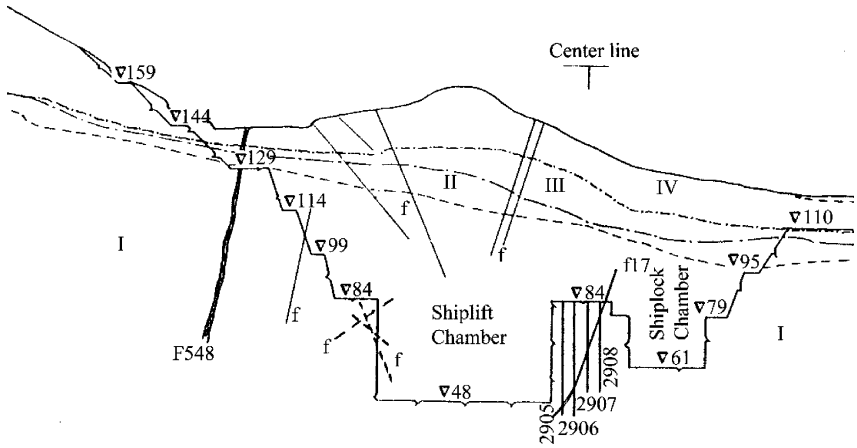


Fig. 8. Rock distribution of a typical section in the temporary shiplock slope.

upright slopes are designed as walls of the navigation chambers for both the shiplocks and the shiplift. For the permanent shiplock, the height of the upright slope is 50–70 m, for the temporary shiplock 29 m, and for the shiplift 34–51 m (see cross-section in Fig. 8). A central rock barrier (or separation block) 55–57 m wide and 50–70 m high is kept between the two channels of the permanent shiplock. Another central rock barrier measuring 16–34 m wide and 23–26 m high is also left between the temporary shiplock and the shiplift chamber.

Such gigantic rock barriers and vertical walls are rare in the history of hydro-power construction. The potential impact of rock deformation on the performance of the navigation facilities was duly recognized in

the early project planning phase. Frequently asked questions pertained to the stability of the vertical walls and the rock barriers after excavation. If they were safe and stable at the time of excavation, would their long-term deformation affect the normal operation of the shiplocks and the shiplift? If they were unstable, should the rock barriers be excavated and replaced by reinforced concrete barriers or kept in place but reinforced to maintain their safety? If reinforcement were feasible, what would be the optimum design and parameters, and son on? To answer these questions, many studies were conducted during the design stage. Most of the questions were satisfactorily answered. However, two conflicting opinions existed regarding the deformation. Some researchers believed that the deformation would be just several centimeters, the same magnitude as that calculated by the elastic finite element analysis, and hence the rock barrier could be stable under some measures of reinforcement, but other researchers insisted that the deformation could be much larger than the calculated value and the rock barrier could be unstable because the barriers might be nearly completely damaged.

The key to answer the above questions lies in understanding the change in rock mass properties due to excavation disturbance and in evaluating the mechanical properties of the disturbed zones. Comprehensive investigations were hence conducted to determine the actual disturbed extent and the mechanical properties, and a finite element analysis of the rock deformation adjacent to the navigation facilities was carried out by the authors, in collaboration with the Yangzte River Resources Commission (the designer), under contract from the China Three Gorges Project Development Corporation (the owner).

The finite element model used for the analysis is shown in Fig. 9, with the axis $x$ being in direction to the downstream and the axis $z$ to the upward vertical. Altogether there are 11,238 nodes and 10,066 block and joint elements in the model. The parameters given by the designer for intact rock and joints are listed respectively in Tables 1 and 2, for the various zones of rock depicted in Fig. 8, along with the loading and in situ conditions. The rocks are considered to satisfy Drucker–Prager's criterion. Two parameters $\alpha$ and $\kappa$ in Drucker–Prager's criterion are determined through letting Drucker–Prager's criterion coincide with Mohr–Coulomb's criterion in the condition of the plane strain (Wang et al., 1982)

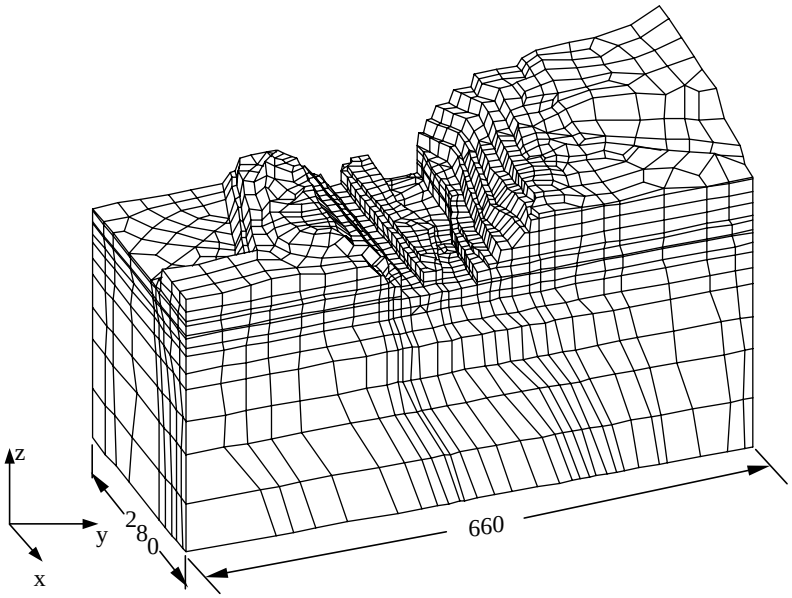


Fig. 9. Finite element model of the temporary shiplock after excavation.

Table 1
Mechanical parameters of rocks

| RC | DW | $d$ (kN/m$^3$) | $E$ (GPa) | $v$ | $\sigma_b$ (MPa) | $C_0$ (MPa) | $f_0$ | $C_r$ (MPa) | $f_r$ |
|---|---|---|---|---|---|---|---|---|---|
| Plagioclase granite | SWF | 27.0 | 40.0 | 0.22 | 1.5 | 1.8 | 1.8 | 0.7 | 1.3 |
| | MW | 26.8 | 15.0 | 0.24 | 1.0 | 1.0 | 1.3 | 0.35 | 1.1 |
| | CHW | 26.5 | 1.0 | 0.30 | 0.0 | 0.1 | 0.7 | 0.07 | 0.7 |

*Note*: RC = rock category, DW = degree of weathering; SWF = slightly weathered and fresh; MW = moderately weathered; CHW = completely and highly weathered.

Table 2
Mechanical parameters of structural planes

| Category | $k_s$ (MPa/m) | $k_n$ (MPa/m) | $C_0$ (MPa) | $f_0$ | $C_r$ (MPa) | $f_r$ | |
|---|---|---|---|---|---|---|---|
| Hard and thin infillings | | 3000 | 7500 | 0.20 | 0.70 | 0.10 | 0.6 |
| Soft structural planes | SWF, MW | 1000 | 2500 | 0.18 | 0.60 | 0.12 | 0.5 |
| | CHW | 1000 | 2500 | 0.12 | 0.40 | 0.07 | 0.35 |

$$\alpha = \frac{tg\phi}{(9 + 12tg^2\phi)^{1/2}}, \quad \kappa = \frac{3C}{(9 + 12tg^2\phi)^{1/2}}. \tag{45}$$

If $C$ and $\phi$ are taken as the peak strength parameters $C_0$ and $\phi_0 = (tg^{-1}f_0)$ in Table 1, respectively, the peak strength surface of Drucker–Prager's criterion can be obtained. For rock joints, we apply Mohr–Coulomb's criterion.

According to the in situ measurement carried out by the designer, the initial geostress field in the slight weathered and fresh rock is characterized by the horizontal stresses being greater than the vertical stress that is approximate to the stress due to the self-weight of rock mass. In computation, the geostress field was hence represented through loading the self-weight in the vertical direction and the following distribution on the boundary of $X = X_{\min}$:

$$\begin{cases} \sigma_x = 4.3982\beta + 0.01168H \ (\text{MPa}), \\ \tau_{xy} = \tau_{zx} = 0 \end{cases} \tag{46}$$

and $Y = Y_{\max}$

$$\begin{cases} \sigma_y = 4.6867\beta + 0.01168H \ (\text{MPa}), \\ \tau_{xy} = \tau_{yz} = 0, \end{cases} \tag{47}$$

respectively, in which $H$ represents the depth and $\beta$ is the reduction factor defined as the ratio of the Young modulus of a rock in the model to the Young modulus of the slightly weathered and fresh rock. The boundaries of $X = X_{\max}, Y = Y_{\min}$ and $Z = Z_{\min}$ are constrained in the normal and free in the tangential.

Staged excavation was simulated in the computation, with all relevant boundaries being constrained in the normal. For each excavation, convergence can be arrived with finite iterations. That means that the entire rock mass in the region would be stable during excavation.

Fig. 10 shows the disturbed zone computed for the rock barrier between the shiplift chamber and the temporary shiplock chamber (see cross-section 3–3 in Fig. 10, and the layout in Fig. 7), for the three cases of elastic analysis ($E$), elasto-plastic analysis (EP) and elasto-brittle-plastic analysis (EBP), respectively. The disturbed zone is defined as a stress-relieved, weakened zone produced by the excavation process, corresponding to the zone of tension and shear damage (Deng et al., 2001). The field measured disturbed zone is also shown in Fig. 10, for comparison purposes, which was determined in the field jointly by the

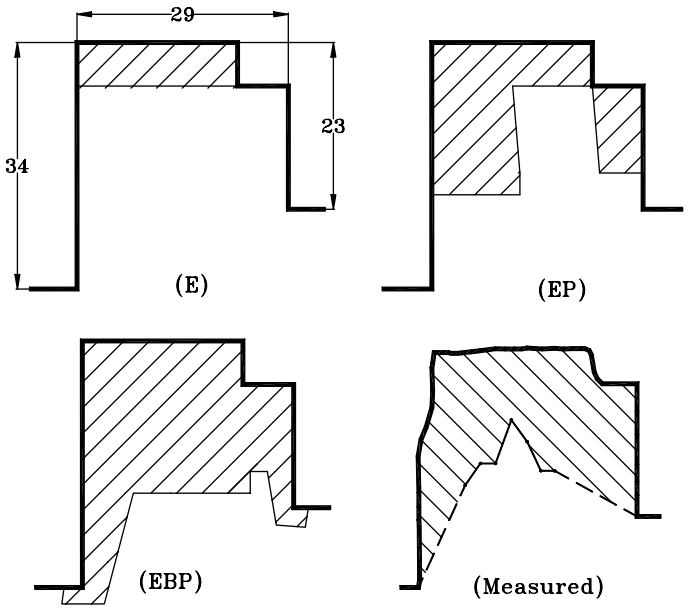


Fig. 10. Damaged zones in the rock barrier.

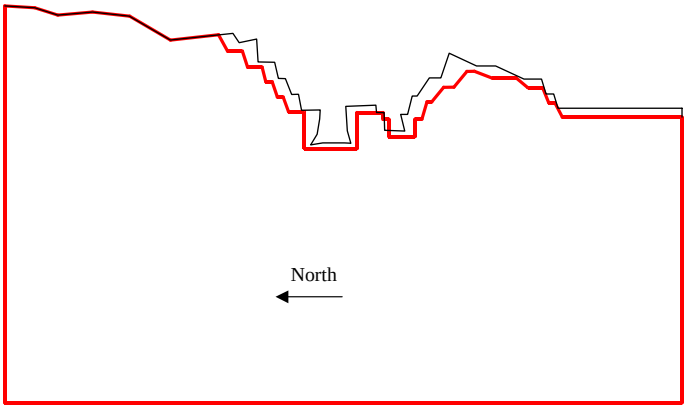


Fig. 11. Deformation of a section after excavation.

cross-hole seismic wave penetration testing and borehole elastic modulus testing (Deng et al., 2001). The results of the brittle-plastic analysis appear to be closest to the field observation, among the results of the three analyses.

Fig. 11 illustrates the deformation of a section after excavation based on the assumption of brittle-plasticity. The rock barrier obviously inclines towards the North. Table 3 lists the deformation of some typical points on the section shown in the Fig. 12 from three constitutive models. The differences of those points far from the rock barrier and the upright walls are small, but the differences of those points—3, 6, 7 and 10, on the tops of the barrier and the upright walls are obvious. The deformations are in the magnitude of centimeter even if the rock mass is regarded as being in the worst case. The displacement measurements in situ has verified these judgments.

Table 3
Deformation of some typical points on the section shown in Fig. 12 (unit: cm)

| Points | *E* | | | EP | | | EBP | | |
|---|---|---|---|---|---|---|---|---|---|
| | Hor[a] | Ver | Tot[b] | Hor | Ver | Tot | Hor | Ver | Tot |
| 1 | 1.45 | 0.65 | 1.59 | 1.46 | 0.65 | 1.60 | 1.47 | 0.65 | 1.61 |
| 2 | 1.82 | 0.47 | 1.88 | 1.83 | 0.47 | 1.89 | 1.81 | 0.50 | 1.87 |
| 3 | 2.05 | −0.04 | 2.05 | 2.08 | 0.04 | 2.08 | 2.23 | 0.26 | 2.24 |
| 4 | 0.66 | 0.16 | 0.68 | 0.65 | 0.15 | 0.66 | 0.65 | 0.13 | 0.66 |
| 5 | −0.58 | 0.60 | 0.83 | −0.59 | 0.58 | 0.83 | −0.60 | 0.57 | 0.83 |
| 6 | −1.37 | 0.63 | 1.51 | −1.43 | 0.65 | 1.58 | −1.53 | 0.84 | 1.74 |
| 7 | −0.59 | 0.80 | 1.00 | −0.55 | 0.82 | 0.99 | −0.37 | 0.89 | 0.97 |
| 8 | −0.65 | 0.79 | 1.02 | −0.67 | 0.77 | 1.03 | −0.69 | 0.80 | 1.06 |
| 9 | −1.04 | 0.62 | 1.21 | −1.05 | 0.61 | 1.21 | −1.06 | 0.63 | 1.23 |
| 10 | −1.90 | 0.46 | 1.95 | −1.91 | 0.46 | 1.97 | −1.99 | 0.54 | 2.06 |
| 11 | −1.93 | 1.14 | 2.24 | −1.94 | 1.13 | 2.25 | −1.94 | 1.15 | 2.25 |

[a] The deformation towards the South is positive (see in Fig. 11).
[b] $\mathrm{Tot} = (\mathrm{Hor}^2 + \mathrm{Ver}^2)^{1/2}$.

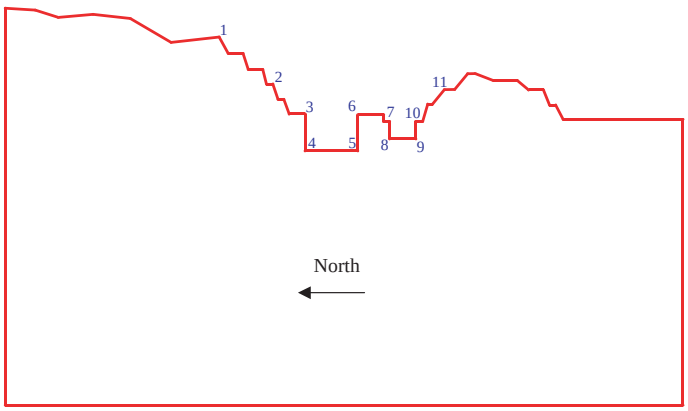


Fig. 12. Some typical points on a section in the model.

Although procedures based on phenomenological models including this study might not simulate strain localization and crack development in rock mass, damaged zones, the degree of damage, the deformation of rock mass, the global stability and many other useful data can be evaluated rather rationally. Zheng et al. (2004) investigated the development of cracks in the rock barrier and the stability.

## 7. Conclusions

This paper proves that, within the framework of the classical theory of plasticity, there is a limit to the rate of softening of a strain-softening material. A procedure for analyzing the abrupt change from the peak strength surface to the residual strength surface is developed, based on the Il'yushin's postulate and the plastic potential theory. The criterion of stability is formulated, which can be used to evaluate the ultimate load of a brittle-plastic body acted by the given load distribution. The analytical and numerical procedure thus developed has been validated with two simple examples, and the engineering application case of a steep rock slope adjacent to the shiplock for the Three Gorges project in China.

Although procedures based on phenomenological models including this study might not simulate some details such as strain localization and crack development in rock mass, damaged zones, the degree of damage, the deformation of rock mass, the global stability and many other useful data can be qualified quite well.

## Acknowledgments

The authors acknowledge the support of the Fund for Excellent Youth of Hubei Provincial Department of Science and Technology and the Fund for Excellent Innovation Team of Hubei Provincial Department of Education.

## References

Ajit, K.M., Sarva, J.S., 1991. Deformation of Elastic Solids. Prentice-Hall.

Atkinson, B.K., 1984. Subcritical crack growth in geological materials. Journal of Geophysical Research 89 (B6), 4077–4114.

Bardet, J.P., 1990. A comprehensive review of strain localization in elastoplastic soils. Computer and Geotechnics 10, 163–188.

Chen, W.F., Han, D.J., 1988. Plasticity for Structural Engineers. Springer-Verlag.

Chiarelli, A.S., Shao, J.F., Hoteit, N., 2003. Modeling of elastoplastic damage behavior of a claystone. International Journal of Plasticity 19 (1), 23–45.

de Borst, R., 1991. Simulation of strain localization: a reappraisal of the Cosserat continuum. Engineering Computations 8, 317–332.

de Borst, R., Muhlhaus, H.B., 1992. Gradient-dependent plasticity: formulation and algorithm aspects. International Journal for Numerical Methods in Engineering 35, 521–539.

de Borst, R., Muhlhaus, H.B, Pamin, J., 1993. Fundamental issues in finite element analysis of localization of deformation. Engineering Computations 10, 99–121.

Dems, K., Mroz, Z., 1985. Stability condition for brittle plastic structure with propagating damage surface. Journal of Structural Mechanics 13, 85–122.

Deng, J.H., Lee, C.F., Ge, X.R., 2001. Characterization of the disturbed zone in a large rock excavation for the Three Gorges Project. Canadian Geotechnical Journal 38 (1), 95–106.

Etienne, F.H., Hoxha, D., Shao, J.F., 1998. A continuum damage constitutive law for brittle rocks. Computer and Geotechnics 22 (2), 135–151.

Fredrich, J.T., Wong, T.F., 1986. Micromechanics of thermally induced cracking in three crustal rocks. Journal of Geophysical Research 91, 12743–12764.

Fredrich, J.T., Evans, B., Wong, T.F., 1989. Micromechanics of the brittle to plastic transition in Carrara marble. Journal of Geophysical Research 94, 4129–4145.

Hajiabdolmajida, V., Kaisera, P.K., Martin, C.D., 2002. Modeling brittle failure of rock. International Journal of Rock Mechanics & Mining Sciences 39, 731–741.

Ju, J.W., 1989. On the energy based coupled elastoplastic damage theories: constitutive modeling and computational aspects. International Journal of Solids and Structures 25 (7), 803–833.

Kemeny, J.M., Cook, N.G.W., 1991. Micromechanics of deformation in rocks. In: Shah, S.P. (Ed.), Toughening Mechanics in Quasi-Brittle Materials. Kluwer Academic, pp. 155–188.

Krajcinovic, D., Vujosevic, M., 1998. Intrinsic failure modes of brittle materials. International Journal of Solids and Structures 35 (19), 2487–2503.

Krajcinovic, D., Mastilovic, S., 1999. Statistical models of brittle deformation: Part I. Introduction. International Journal of Plasticity 15 (4), 401–426.

Litewka, A., Debinski, J., 2003. Load-induced oriented damage and anisotropy of rock-like materials. International Journal of Plasticity 19 (12), 2171–2191.

Liu, W.Z., Xu, B.Y., 1989. Stability condition for brittle-plastic symmetric thick-walled shell structures. Acta Mechanica Solida Sinica 2, 71–76.

Lo, K.Y., Lee, C.F., 1973. Stress analysis and slope stability in strain-softening material. Géotechnique 23, 1–11.

Martin, C.D., Chandler, N.A., 1994. The progressive failure of Lac du Bonnet granite. International Journal of Rock Mechanics and Mining Sciences 31, 643–659.

Mastilovic, S., Krajcinovic, D., 1999. Statistical models of brittle deformation: Part II. Computer simulations. International Journal of Plasticity 15 (4), 427–456.

Muhlhaus, H.B., Vardoulakis, I., 1987. The thickness of shear bands in granular materials. Géotechnique 37, 271–283.
Pietruszczak, S., Xu, G., 1995. Brittle response of concrete as a localization problem. International Journal of Solids and Structures 32 (11), 1517–1533.
Pijaudier-Cabot, G., Bazant, Z.P., 1987. Nonlocal damage theory. Journal of Engineering Mechanics, ASCE 113, 1512–1533.
Regueiro, R.A., Borja, R.I., 2000. A finite model of localized deformation in frictional material taking a strong discontinuity approach. Finite Element in Analysis and Design 33, 283–315.
Roy, A.B., Marc, G.D., Frank, P.T., 2003. Nonlocal implicit gradient-enhanced elasto-plasticity for the modelling of softening behaviour. International Journal of Plasticity 19 (4), 403–433.
Sammis, C.G., Ashby, M.F., 1986. The failure of brittle porous solids under compressive stress states. Acta Metallurgica 34 (3), 511–526.
Steif, P.S., 1984. Crack extension under compressive loading. Engineering Fracture Mechanics 20 (3), 463–473.
Wan, R., Chan, D., Morgenstern, N., 1992. Modeling discontinuous behavior and fault formation in geomaterials. In: Conference on Fractured and Jointed Rock Masses, June 3–5, Lake Tahoe, pp. 328–334.
Wang, Y., Dussealt, M.B., 1994. Stress around a circular opening in an elastoplastic porous medium subjected to repeated hydraulic loading. International Journal of Rock Mechanics and Mining Sciences 31, 597–616.
Wang, R., Xong, Z.H., Huang, W.B., 1982. Introduction of Plasticity Mechanics. The Science Press.
Wawersik, W.R., Brace, W.F., 1971. Post-failure behavior of granite and diabase. Rock Mechanics 3, 61–85.
Wells, G.N., Sluys, L.J., 2001. Three-dimensional embedded discontinuity model for brittle fracture. International Journal of Solids and Structures 38, 897–913.
Wong, T.F., 1982. Micromechanics of faulting in Westerly granite. International Journal of Rock Mechanics and Mining Sciences 19, 49–62.
Zhang, W., Subhash, G., 2001. An elastic–plastic-cracking model for finite element analysis of indentation cracking in brittle materials. International Journal of Solids and Structures 38 (34), 5893–5913.
Zheng, H., Liu, D.F., Lee, C.F., Yue, Z.Q., 2004. A sophisticated node-pair model for interface problems. Computers and Geotechnics 31 (2), 137–154.
Zienkiewicz, O.C., Taylor, R.L., 1991, fourth ed.The Finite Element Method, vol. 2 McGraw-Hill Book Company.